DINAME 2017 - Proceedings of the XVII International Symposium on Dynamic Problems of Mechanics
A. T. Fleury, D. A. Rade, P. R. G. Kurka (Editors), ABCM, São Sebastião, SP, Brazil, March 5-10, 2017.

Dynamical Stability Analysis of a 2-DOF SMA Oscillator

Guilherme Vieira Rodrigues [1], Guilherme Luiz Torres Mendonça [2], Alberto Paiva [2] and Marcelo Amorim Savi [1]

[1] Universidade Federal do Rio de Janeiro – COPPE – Department of Mechanical Engineering
Center for Nonlinear Mechanics – MECANON – Rio de Janeiro – RJ – Brazil – 21.941.972
guilherme_@live.co.uk, savi@mecanica.ufrj.br

[2] Universidade Federal Fluminense – Volta Redonda School of Engineering – Department of Mechanical Engineering
420 Trabalhadores Av. – Volta Redonda − RJ – Brazil – 27.255-125
guilhermeid@hotmail.com, paiva.ufrj@gmail.com

*Abstract: The hysteretic behavior inherent to intelligent materials turns their respective formulation intrinsically nonlinear, enabling plentiful dynamical responses, ranging from periodic to chaotic solutions. This paper aims to discuss the dynamical stability of a two-degree of freedom sketch with Shape Memory Alloy (**SMA**) restoring elements, considering a polynomial constitutive model. The numerical results consider stable/unstable points' identification, besides mapping the influence of different temperature of the **SMA** elements by means of basins of attraction.*

Keywords: Nonlinear dynamics, basins of attraction, stability analysis, chaos.

INTRODUCTION

While modeling most of nowadays applications, simple mechanical sketches may provide suitable solutions for practical purposes. Nevertheless, when the **SMA** behavior is incorporated to even simple physical models, the resulting mathematical formulation is highly nonlinear – especially in time-varying problems, unveiling all the dynamical richness of this kind of system, including coexistence of multiple solutions, jump phenomena, interesting topologies and bifurcations cascades that lead to non-regular (chaotic) responses. For a successful designing of mechanical systems using **SMA**, a thorough comprehension of the smart structure response is imperative.

Updated review works on **SMA** constitutive models (for instance, Cisse et al., 2016) report an increasing number of new proposed formulations, besides those well-established in the literature. Each of them has its advantages and drawbacks, depending on the scope of application. Moreover, there are some desirable characteristics that should be met, concerning: number of model parameters and their physical meanings; friendly mathematical formulation; easy numerical implementation, besides being all-inclusive.

Savi (2015) provides a review of dynamical applications involving **SMA** systems, highlighting the use of different constitutive models to describe the shape memory thermomechanical behavior. Some of the research groups working on the subject are presented, as follows.

The polynomial model proposed by Falk (1980), based on the Landau-Devonshire-Ginzburg theory to describe the **SMA** first-order phase transitions, has inspired a number of applied works, such as: Savi & Braga (1993); Savi & Pacheco (2002); Machado et al. (2003); Rodrigues et al. (2015). The great advantage of this constitutive model is its simplicity. As a matter of fact, the application of the Falk model to dynamical systems, turn its description similar to the Duffing oscillator, despite of having one more stable equilibrium point under specific parameter conditions. Two main drawbacks may be assigned to this model: it does not take dissipation into account (this feature can be overcome introducing a dashpot in parallel with the **SMA** restoring element) and it does not consider the temperature induced twinned martensite variant and, thus, is not able to capture the shape memory effect.

Paiva et al. (2005) proposed a constitutive model based upon the original model with internal constraints formulated by Fremond (1987). Savi and co-workers have applied this model in different mechanical archetypes for several purposes, such as in the following references: Savi et al. (2008); Santos & Savi (2009); Savi et al. (2011); Silva et al. (2013); Oliveira et al. (2014). The main advantage of the constitutive model used in these works is that it enables complex thermomechanical behaviors description as, for example: controlled temperature transformations and internal subloops, while dissipating energy. Its main drawback consists of a slight softening effect for a strain driven condition (exactly the one which takes place in dynamical analyses).

Bernardini & Pence (2002) introduced some amendments in the original model proposed by Ivshin & Pence (1994), in order to apply this model into dynamical systems. Since then, different authors have used the modified model to conduct nonlinear analyses, as follows. Wiercigroch and co-workers applied this constitutive theory to model an **SMA** oscillator with impact (Sitnikova et al. 2008, 2012). An italian research group, in collaboration with other authors, has exhaustively employed this model to simulate different mechanical system configurations, such as in the following articles: Bernardini & Vestroni (2000); Bernardini & Vestroni (2003); Lacarbonara & Vestroni (2012); Bernardini & Rega (2005; 2011); Litak et al. (2013); Carpineto et al. (2014); Piccirillo et al. (2015).

There are other works on **SMA** dynamical applications using different constitutive models, as follows. Lagoudas et al. (2004) and Machado et al. (2009) used a constitutive model adapted from Boyd & Lagoudas (1996). Enemark et al. (2014) conducted a numerical-experimental study, where the numerical results explore the constitutive model conceived by Brinson (1993). Seelecke (2002) explores the effect of change in temperature of the **SMA** element under torsional mechanical vibration, using the constitutive model formulated by Achenbach & Muller (1982).

This article investigates the dynamical stability of the natural response of a 2-DOF **SMA** oscillator, considering different **SMA** elements' temperature. The **SMA** constitutive behavior is described by Falk's model (Falk, 1980). The resulting set of coupled nonlinear ordinary differential equations is solved using a fourth-order Runge-Kutta scheme. The numerical results involve the identification of stable/unstable equilibrium points and their analogy with the respective potential energy surfaces and state-space orbits for conservative cases. Besides that, basins of attraction for non-conservative cases are mapped with two purposes: analyze the basin of attraction evolution varying the **SMA** element temperatures.

MATHEMATICAL MODELING

This section comprises the dynamical physical model and its respective mathematical formulation through the Lagragean formalism, incorporating the **SMA** polynomial constitutive model. Aiming an optimized numerical implementation, the resulting set of ordinary differential equations of motion is put in a dimensionless form.

Figure 1 presents the physical model for a two-degree of freedom oscillator with **SMA** restoring elements, where: m_1 and m_2 are lumped masses with linear absolute displacements denoted by $u_1(t)$ and $u_2(t)$, respectively; c_1, c_2 and c_3 are damping coefficients, while the thermomechanical behavior of the **SMA** elements is described by the polynomial constitutive model proposed by Falk (1980), which free-energy expression is presented in Eq. (1).

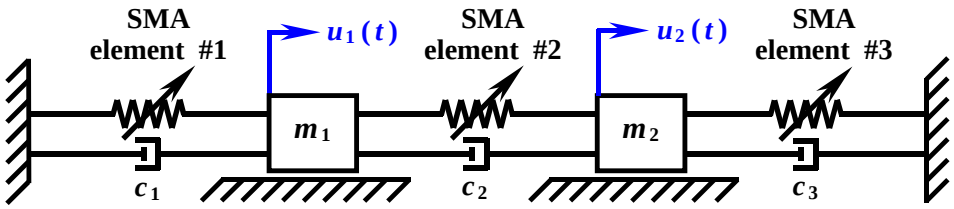

Figure 1 – Two-degree of freedom SMA oscillator physical model.

$$\psi(\varepsilon, T) = \frac{a(T - T_M)}{2}\varepsilon^2 - \frac{b}{4}\varepsilon^4 + \frac{e}{6}\varepsilon^6 \tag{1}$$

where a, b and $e = b^2/4a(T_A - T_M)$ are material parameters; ψ is the *Helmholtz* free-energy potential, which is function of the observable variables ε and T, meaning the uniaxial strain and the absolute temperature; whereas T_A and T_M are the beginning transformation temperatures for austenite and martensite formation, respectively.

Euler-Lagrange's equation in its general form is given by Eq. (2), where: K is the total kinetic energy of the system; V is the total potential energy, while ϕ is the total dissipation energy. Besides, $\underline{q}$ is the generalized coordinates' vector; $\underline{Q}(t)$ is the generalized forcing vector; t is the independent variable time; whereas $(\bullet)$ corresponds to $(\bullet) = d(\ )/dt$.

$$\frac{d}{dt}\left(\frac{\partial K}{\partial \dot{\underline{q}}}\right) - \frac{\partial K}{\partial \underline{q}} + \frac{\partial V}{\partial \underline{q}} = \underline{Q}(t) - \frac{\partial \phi}{\partial \dot{\underline{q}}} \qquad \text{where } \underline{q} = \begin{Bmatrix} u_1 \\ u_2 \end{Bmatrix} \tag{2}$$

The total kinetic energy (K) may be obtained by the summation ($K = K_1 + K_2$) of the translational kinetic energy for blocks m_1 and m_2, given by:

$$K(\dot{u}_1, \dot{u}_2) = K_1 + K_2 = \frac{m_1(\dot{u}_1)^2}{2} + \frac{m_2(\dot{u}_2)^2}{2} \tag{3}$$

The **SMA** elements are assumed as slender bars of cross sectional area A and length L, undergoing tension/compression. Thus, their uniaxial strain, under small deformations assumption, may be taken as: $\varepsilon_n = \Delta u_n / L$, where Δu_n (n = 1,2,3) represents the elongation of each **SMA** element. Considering all three elements with the same geometrical and material parameters, the total potential energy (V) may be obtained by the summation ($V = V_1 + V_2 + V_3$) of the strain energy associated with each **SMA** restoring element, given as follows:

$$V\left(u_1,u_2\right)=V_1+V_2+V_3=A\left[\frac{a\left(T_1-T_M\right)}{2}\left(\frac{u_1}{L}\right)^2-\frac{b}{4}\left(\frac{u_1}{L}\right)^4+\frac{e}{6}\left(\frac{u_1}{L}\right)^6\right]+$$
$$+A\left[\frac{a\left(T_2-T_M\right)}{2}\left(\frac{u_2-u_1}{L}\right)^2-\frac{b}{4}\left(\frac{u_2-u_1}{L}\right)^4+\frac{e}{6}\left(\frac{u_2-u_1}{L}\right)^6\right]+A\left[\frac{a\left(T_3-T_M\right)}{2}\left(\frac{u_2}{L}\right)^2-\frac{b}{4}\left(\frac{u_2}{L}\right)^4+\frac{e}{6}\left(\frac{u_2}{L}\right)^6\right] \tag{4}$$

Analogously, the total dissipation energy (ϕ) is given by the summation ($\phi=\phi_1+\phi_2+\phi_3$) of the dissipation energy associated with each of the three dashpots, as follows:

$$\phi\left(\dot{u}_1,\dot{u}_2\right)=\phi_1+\phi_2+\phi_3=\frac{c_1\dot{u}_1^{\,2}}{2}+\frac{c_2\left(\dot{u}_2-\dot{u}_1\right)^2}{2}+\frac{c_3\dot{u}_2^{\,2}}{2} \tag{5}$$

Proceeding with the appropriate derivations assigned in Eq. (2) and neglecting external disturbances, i.e. $\underline{Q}(t)=0$, after some algebraic manipulation, the following equations of motion for the 2-DOF **SMA** oscillator arises:

$$\begin{cases} m_1L^5\,\ddot{u}_1+\left(c_1+c_2\right)L^5\,\dot{u}_1-c_2\,L^5\,\dot{u}_2+a\,A\,L^4\left[\left(T_1-T_M\right)u_1-\left(T_2-T_M\right)\left(u_2-u_1\right)\right]- \\ \qquad -b\,A\,L^2\left[u_1^{\,3}-\left(u_2-u_1\right)^3\right]+e\,A\left[u_1^{\,5}-\left(u_2-u_1\right)^5\right]=0 \\ m_2\,L^5\,\ddot{u}_2-c_2\,L^5\,\dot{u}_1+\left(c_2+c_3\right)L^5\,\dot{u}_2+a\,A\,L^4\left[\left(T_2-T_M\right)\left(u_2-u_1\right)+\left(T_3-T_M\right)u_2\right]- \\ \qquad -b\,A\,L^2\left[\left(u_2-u_1\right)^3+u_2^{\,3}\right]+e\,A\left[\left(u_2-u_1\right)^5+u_2^{\,5}\right]=0 \end{cases} \tag{6}$$

To obtain the dimensionless differential equations of motion, consider the new variables: $\tau=\omega\,t$ as the new independent variable, where ω is an angular frequency concerning a reference value; $\theta_n=T_n/T_M$ (n = 1,2,3) is the dimensionless temperature; while $U_1=u_1/L$ and $U_2=u_2/L$ are the new dimensionless displacements for masses m_1 and m_2, respectively.

At this point, the original variables $u_1(t)$ and $u_2(t)$ and their derivatives are substitued for the new dimensionless variables $U_1(\tau)$ and $U_2(\tau)$, regarding that: $U_m=U_m\left(\tau(t)\right)$ (for m = 1,2). Therefore, by applying the chain's rule, $\dot{u}_m=L\,\omega\,U_m^{'}$ and $\ddot{u}_m=L\,\omega^2\,U_m^{''}$, where: $U_m^{'}=d\,U_m/d\,\tau$. Moreover, the first of Eqs. (6) related to m_1 is simplified by the factor $m_1L^5\,\omega^2$, while the second equation related to m_2 is simplified by the factor $m_2\,L^5\,\omega^2$. After all these algebraic procedures, eventually, the following set of second-order ordinary differential equations arises:

$$\begin{cases} U_1^{''}+\alpha\,U_1^{'}-\beta\,U_2^{'}+\phi\left[\left(\theta_1-1\right)U_1-\left(\theta_2-1\right)\left(U_2-U_1\right)\right]-\gamma\left[U_1^{\,3}-\left(U_2-U_1\right)^3\right]+\eta\left[U_1^{\,5}-\left(U_2-U_1\right)^5\right]=0 \\ U_2^{''}-\xi\,U_1^{'}+\mu\,U_2^{'}+\rho\left[\left(\theta_2-1\right)\left(U_2-U_1\right)+\left(\theta_3-1\right)U_2\right]-\varphi\left[\left(U_2-U_1\right)^3+U_2^{\,3}\right]+\lambda\left[\left(U_2-U_1\right)^5+U_2^{\,5}\right]=0 \end{cases} \tag{7}$$

Concerning the new dimensionless parameters, they are related to the original ones as follows:

$$\alpha=\frac{c_1+c_2}{m_1\,\omega}\qquad \beta=\frac{c_2}{m_1\,\omega}\qquad \phi=\frac{a\,A\,T_M}{m_1\,L\,\omega^2}\qquad \gamma=\frac{b\,A}{m_1\,L\,\omega^2}\qquad \eta=\frac{e\,A}{m_1\,L\,\omega^2}$$
$$\xi=\frac{c_2}{m_2\,\omega}\qquad \mu=\frac{c_2+c_3}{m_2\,\omega}\qquad \rho=\frac{a\,A\,T_M}{m_2\,L\,\omega^2}\qquad \varphi=\frac{b\,A}{m_2\,L\,\omega^2}\qquad \lambda=\frac{e\,A}{m_2\,L\,\omega^2} \tag{8}$$

In addition to that, consider: $m_1=m_2=1$ that results in: $\beta=\xi$; $\phi=\rho$; $\gamma=\varphi$; $\eta=\lambda$. Besides that, if the reference angular frequency is defined as: $\omega=\sqrt{a\,A\,T_M/m_1\,L}$, thus: $\phi=\rho=1$.

For the purpose of numerical implementation via fourth-order Runge-Kutta method, it is necessary to convert the original system consisting of two second-order ordinary differential equations (Eqs. 7) into a new set of first-order ordinary differential equations with four equations (Eqs. 9). Hence, consider a new variables' change, such that: $U_1 = x_0$; $U_1^{'} = x_1$; $U_2 = x_2$; $U_2^{'} = x_3$, where the new derivatives denoted by $(\bullet)$ correspond to $(\bullet) = d(\ )/d\tau$. Finally, the dynamical governing differential equations in their ultimate form are given by:

$$\begin{cases} \dot{x}_0 = x_1 \\ \dot{x}_1 = -\alpha\, x_1 + \beta\, x_3 - \left[(\theta_1 - 1)\, x_0 - (\theta_2 - 1)(x_2 - x_0)\right] + \gamma\left[x_0^{\,3} - (x_2 - x_0)^3\right] - \eta\left[x_0^{\,5} - (x_2 - x_0)^5\right] \\ \dot{x}_2 = \dot{x}_3 \\ \dot{x}_3 = \beta\, x_1 - \mu\, x_3 - \left[(\theta_2 - 1)(x_2 - x_0) + (\theta_3 - 1)\, x_2\right] + \gamma\left[(x_2 - x_0)^3 + x_2^{\,3}\right] - \eta\left[(x_2 - x_0)^5 + x_2^{\,5}\right] \end{cases} \tag{9}$$

NUMERICAL RESULTS

This section shows the numerical results considering the free response of the 2-DOF proposed model. The dynamical system parameters used in all simulations along this paper are presented in Tab. 1, except for the dimensionless temperatures (θ_1, θ_2, θ_3) that will be varied during the simulations.

Table 1 – Dynamical system parameters.

$\alpha = \beta = \mu$	γ	η
0.10	1.30 x 10^3	4.70 x 10^5

From previous works on this subject (Savi & Pacheco 2002; Machado et al. 2003; Rodrigues et al. 2015), it is well-known that there are three distinct temperature ranges of the **SMA** element with different qualitative behaviors. These three conditions refer to: low temperature condition ($T < T_M$ or $\theta < 1.0$); intermediate temperature condition ($T_A < T < T_M$ or $1 < \theta < 1.9$) and high temperature condition ($T > T_A$ or $\theta > 1.9$).

Figure 2 presents a stability analysis for these three conditions, displayed by columns, considering the three **SMA** elements with the same temperature. The temperature of the elements is indicated right above the figures. Figures 2(a), 2(b) and 2(c) show the equilibrium points identification for the conservative case (i.e. $\alpha = \beta = \mu = 0$), by letting $\{\dot{x}\} = \{f(x_0, x_1, x_2, x_3)\} = \{0\}$ in Eq. (9), together with their classification. Figures 2(d), 2(e) and 2(f) display the potential energy surface, which can be inferred from Eq. (4), as a function of dimensionless displacements (x_0, x_2). In Fig. 2(d), there are six wells associated with six stable equilibrium points identified in Fig. 2(a). Notice that, in Fig 2(a), there is a distinction between unstable and pseudostable points, where the first is associated with two unstable directions, while the second is related to one stable and one unstable direction. This analysis is stemmed from the evaluation of the eigenvalues of the *Jacobian* matrix A_{ij} given by $A_{ij} = \partial f_i / \partial \bar{x}_j$ for $(i, j = 0,1,2,3)$ obtained from Eq. (9), where unstable points exhibit four real eigenvalues (being two of them positive), while pseudostable points exhibit two imaginary and two real eigenvalues (being one of them positive). Figures 2(g), 2(h) and 2(i) illustrate conservative state-space orbits in the subspace $x_0 \times x_2$ for different energy levels. The equilibrium points are reproduced from Fig. 2(a) and the bold lines indicate homoclinic paths. Figures 2(j), 2(k) and 2(l) show the basins of attraction for each case (for null initial velocity conditions, i.e. $x_1 = x_3 = 0$). Again, the equilibrium points are reproduced from Fig. 2(a). Each color is associated with one specific stable equilibrium point. In Figs 2(j) and 2(k), there are densely colored central regions related to different equilibrium points, surrounded by a messy region with a lamellar fractal structure. It is interesting to notice the analogy with the stability analysis of a 1-DOF **SMA** oscillator with the same polynomial Falk model (Savi & Pacheco, 2002), regarding a dynamical richness increase. All interpretations provided here apply for the three temperature conditions.

Next, considering the three reference conditions analyzed in Fig. 2, the basin of attraction evolution is scrutinized through temperature variation of the **SMA** elements. For each of the three reference conditions, the temperature of the left, central and write **SMA** element is varied, migrating from one temperature range to another.

Figure 3 considers the low temperature condition ($\theta_1 = \theta_2 = \theta_3 = 0.8$) as a reference condition. In the first column, the temperature of the left **SMA** element is varied; in the second column, the temperature of the central **SMA** element is varied and in the third column, the temperature of the right **SMA** element is varied.

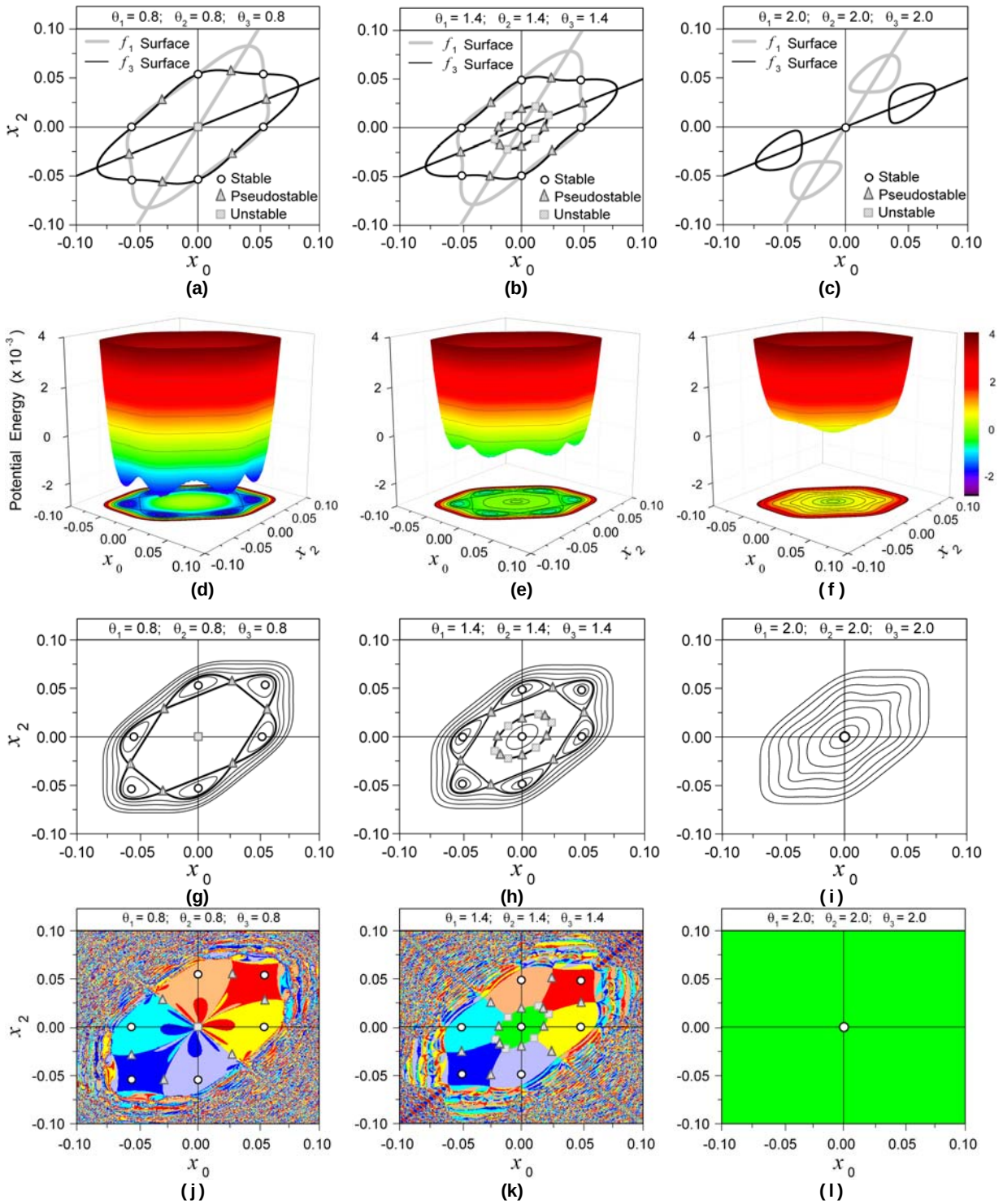

Figure 2 – Stability analysis for 2-DOF oscillator with different SMA element temperatures.

	$\theta_1 = \theta_2 = \theta_3 = 0.8$	$\theta_1 = \theta_2 = \theta_3 = 1.4$	$\theta_1 = \theta_2 = \theta_3 = 2.0$
Equilibrium points	**(a)**	**(b)**	**(c)**
Potential energy × displacements diagram	**(d)**	**(e)**	**(f)**
Conservative state-space orbits	**(g)**	**(h)**	**(i)**
Basins of attraction	**(j)**	**(k)**	**(l)**

In Fig. 3, while increasing the left **SMA** element temperature, the regions orange and light blue – associated with the calculated stable equilibrium points $(x_0, x_2) = (0; \pm 0.054)$ – grow (Figure 3d for $\theta_1 = 1.4$; $\theta_2 = \theta_3 = 0.8$), until they cover all the subspace (Figure 3g for $\theta_1 = 2.0$; $\theta_2 = \theta_3 = 0.8$). The physical interpretation of this behavior is that, when the left **SMA**

element is heated above T_A, its stiffness increases (approaching a linear behavior) and the left mass m_1 oscillates around $x_0 = 0$, while the right mass m_2 oscillates around either a positive position $x_2 = 0.054$ or a negative position $x_2 = -0.054$, due to the influence of the central and write low temperature **SMA** elements acting on mass m_2. While increasing the right **SMA** element temperature, a symmetric behavior takes place, the regions cyan and yellow – related to the calculated stable equilibrium points $(x_0, x_2) = (\pm 0.054;\ 0)$ – grow (Figure 3f for $\theta_1 = \theta_2 = 0.8;\ \theta_3 = 1.4$), until they cover all the subspace (Figure 3i for $\theta_1 = \theta_2 = 0.8;\ \theta_3 = 2.0$). But this time, the right mass m_2 oscillates around $x_2 = 0$ and the left mass m_1 oscillates around either a positive or a negative position, due to the influence of the left and central low temperature **SMA** elements acting on mass m_1. Finally, analyzing the central **SMA** element temperature increase, the regions red and blue – associated with the calculated stable equilibrium points $(x_0, x_2) = (0.054;\ 0.054)$ and $(x_0, x_2) = (-0.054;\ -0.054)$, respectively – grow (Figure 3e for $\theta_1 = 0.8;\ \theta_2 = 1.4;\ \theta_3 = 0.8$), until they cover all the subspace (Figure 3h for $\theta_1 = 0.8;\ \theta_2 = 2.0;\ \theta_3 = 0.8$). In this case, both masses oscillate around either a positive or a negative position, since the left **SMA** element acting on mass m_1 and the right **SMA** element acting on mass m_2 – both at low temperatures – make them oscillate out of their neutral position.

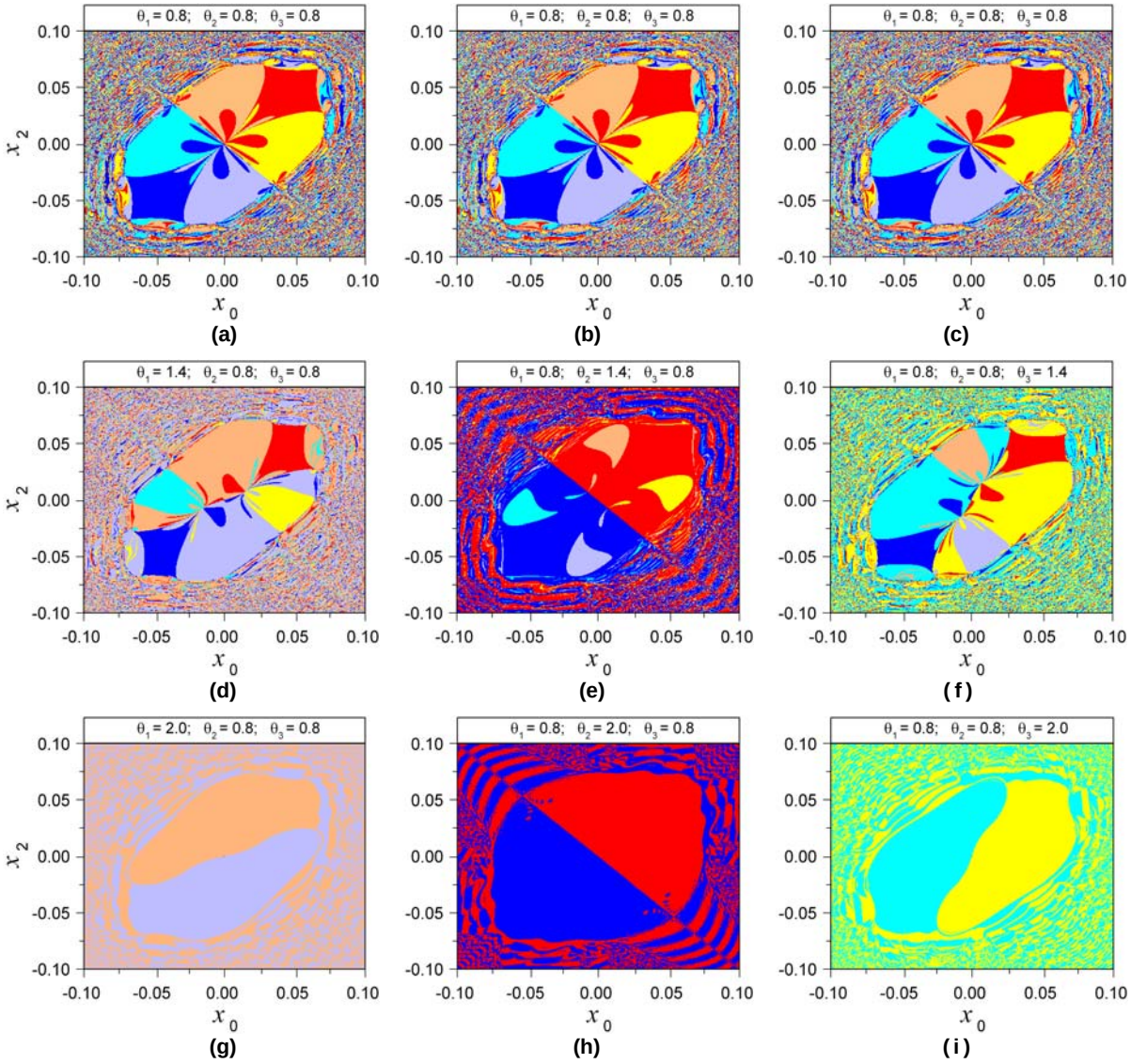

Figure 3 – Basin of attraction evolution varying the SMA elements temperature. (considering the low temperature $\theta = 0.8$ for all three SMA elements as a reference condition).

	Varying the first SMA element	Varying the second SMA element	Varying the third SMA element
Low temperature	**(a)**	**(b)**	**(c)**
Intermediate temperature	**(d)**	**(e)**	**(f)**
High temperature	**(g)**	**(h)**	**(i)**

Figure 4 considers the intermediate temperature condition ($\theta_1 = \theta_2 = \theta_3 = 1.4$) as a reference condition. The **SMA** elements temperature variation follows the same pattern of Fig. 3.

While increasing each of the **SMA** elements temperature (left, central and right), the dynamical standard of predominant regions together with their respective stable equilibrium points remains the same of Fig. 3 analysis, except for the emergence of a new central region in green – associated with low energy levels around the new stable equilibrium point $(x_0, x_2) = (0; 0)$. While decreasing the **SMA** elements temperature from the reference condition, this central region in green fades away. Besides that, for the outermost **SMA** elements temperature reduction – the left one for example (Fig 4a) – the light blue and orange regions – related to the calculated stable equilibrium points $(x_0, x_2) = (0; -0.054)$ and $(x_0, x_2) = (0; 0.054)$, respectively – shrink, at the expense of other regions (blue, cyan, red and yellow) enlargement. The physical interpretation of this behavior is that, when the left **SMA** element is cooled below T_M, the situations where the mass m_1 oscillates around its neutral position ($x_0 = 0$) become less stable than the other four. For the right **SMA** element temperature reduction (Fig 4c), the interpretation is analogous but symmetric. On the other hand, for the central **SMA** element temperature reduction, the red and blue regions shrink, while the other four regions expand themselves. The physical interpretation, in this case, is exactly the opposite of the previous case where one of the outermost **SMA** elements is cooled below T_M. In this case, the situations where both masses oscillate around either a positive or a negative position become less stable than the other four (light blue, cyan, yellow and orange).

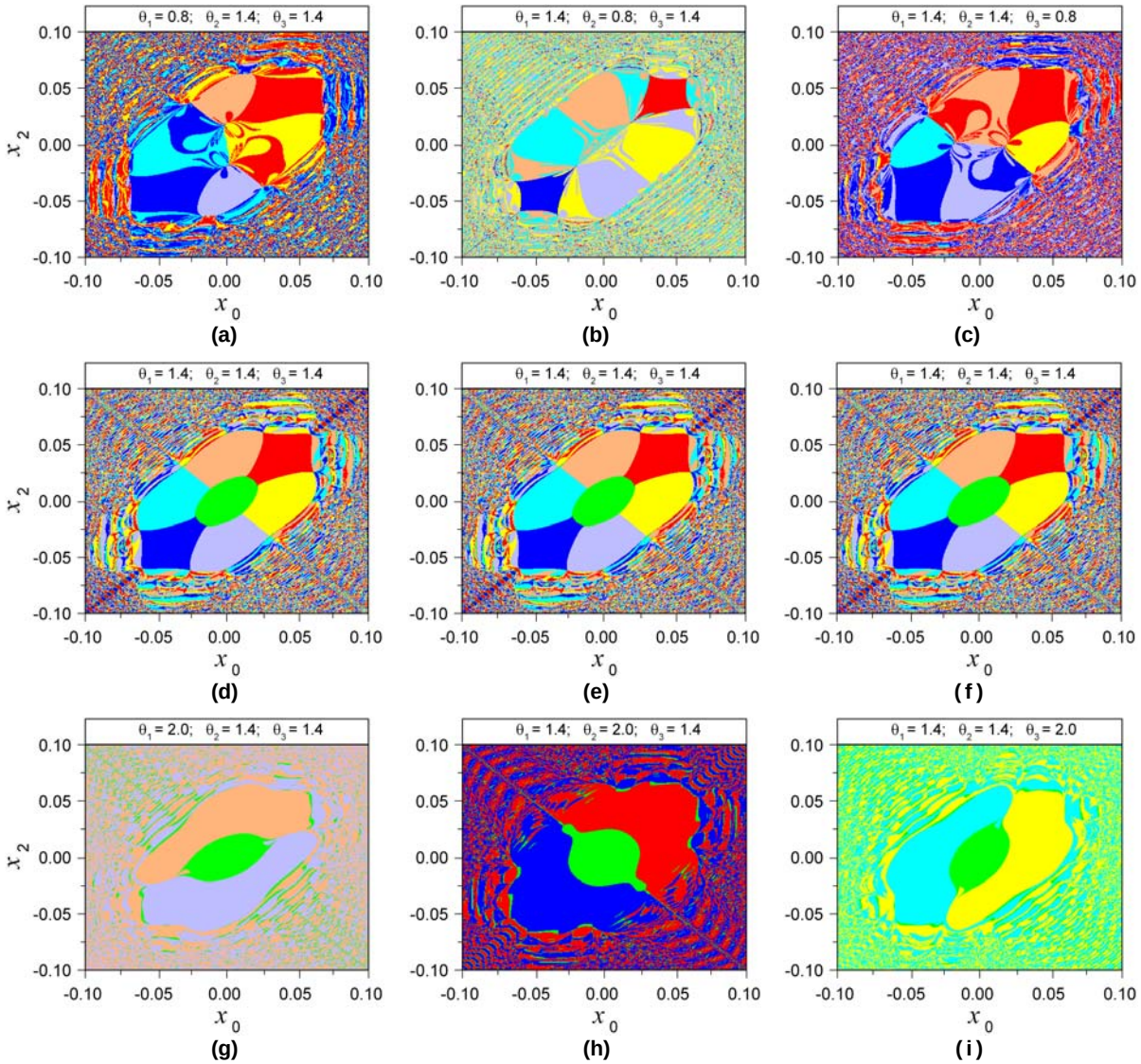

Figure 4 – Basin of attraction evolution varying the SMA elements temperature.
(considering the intermediate temperature $\theta = 1.4$ for all three SMA elements as a reference condition).

	Varying the first SMA element	Varying the second SMA element	Varying the third SMA element
Low temperature	**(a)**	**(b)**	**(c)**
Intermediate temperature	**(d)**	**(e)**	**(f)**
High temperature	**(g)**	**(h)**	**(i)**

Figure 5 considers the high temperature condition ($\theta_1 = \theta_2 = \theta_3 = 2.0$) as a reference condition. Again the **SMA** elements temperature variation follows the same pattern of Fig. 3.

While decreasing **SMA** elements temperature from the high temperature reference condition, there is a gradual reduction of the green region – associated with the stable equilibrium point $(x_0, x_2) = (0; 0)$. However, even for the cases where one of the **SMA** elements is at a low temperature ($\theta = 0.8$), there is still some green region (Figs. 5a, 5b and 5c), due to the other two **SMA** elements at a high temperature ($\theta = 2.0$). While analyzing the spatial influence depending on which **SMA** element is cooled, the dynamical standard of predominant regions together with their respective stable equilibrium points remains the same of Fig. 4 analysis, except for the disappearance of the inhibited regions of Fig. 4. For instance, compare Figs. 4(a), 4(b) and 4(c) with Figs. 5(a), 5(b) and 5(c), where the predominant regions of Fig. 4 repeat themselves in Fig. 5. Another interesting point concerns the highly fractal lamellar structure for the low temperature cases, especially in Figs. 5(a) and 5(c).

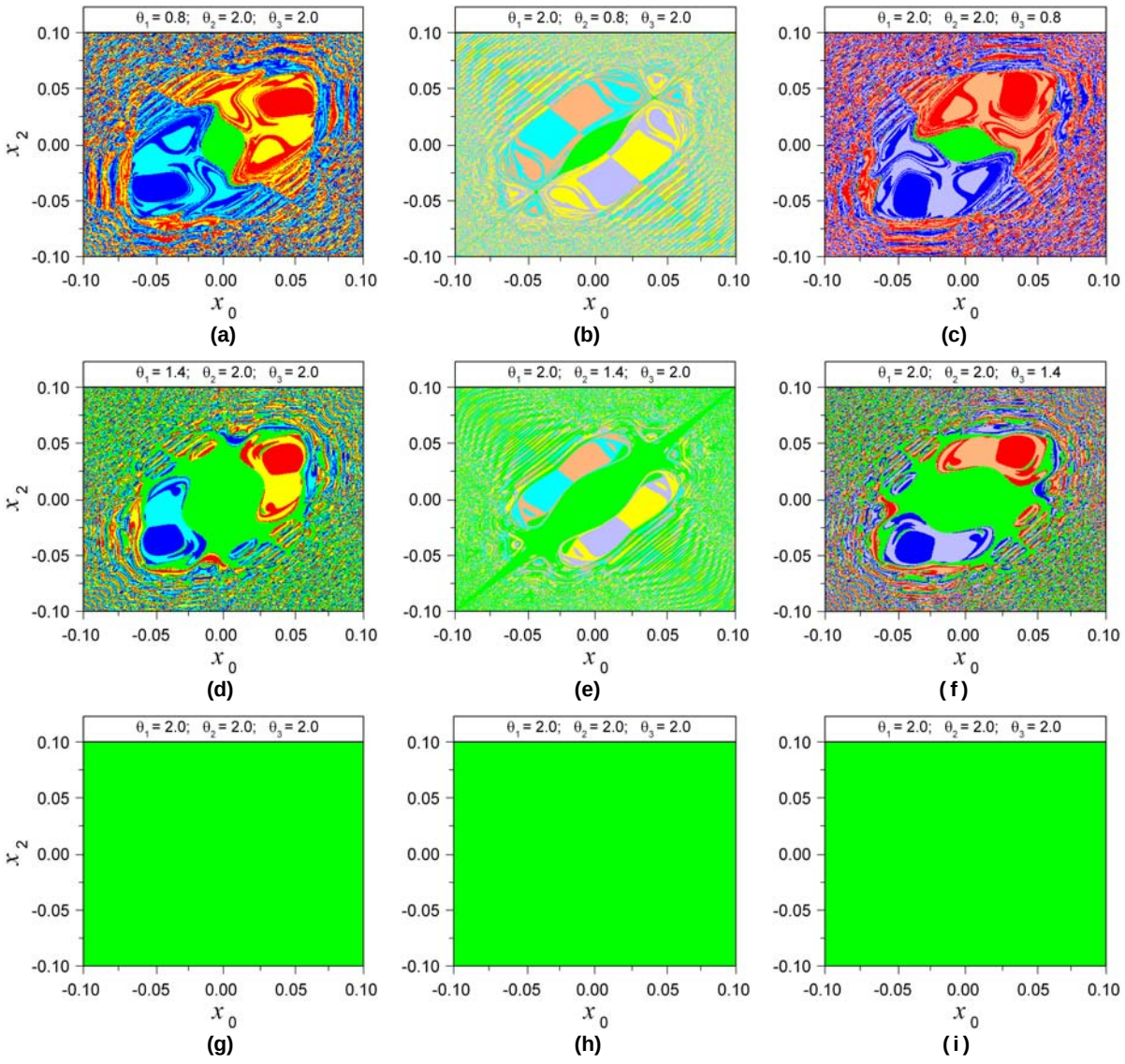

Figure 5 – Basin of attraction evolution varying the SMA elements temperature. (considering the high temperature $\theta = 2.0$ for all three SMA elements as a reference condition).

	Varying the first SMA element	Varying the second SMA element	Varying the third SMA element
Low temperature	**(a)**	**(b)**	**(c)**
Intermediate temperature	**(d)**	**(e)**	**(f)**
High temperature	**(g)**	**(h)**	**(i)**

Concerning the equilibrium points stability analysis, consider the potential energy surface, as a function of dimensionless displacements (x_0, x_2) for: $\theta_1 = 1.4$; $\theta_2 = 0.8$; $\theta_3 = 1.4$ (Fig. 6b) Again, six wells associated with six stable equilibrium points are identified; however, four of them: $(x_0, x_2) = (-0.004;\ 0.049)$; $(x_0, x_2) = (0.004;\ -0.049)$; $(x_0, x_2) = (-0.049;\ 0.004)$ and $(x_0, x_2) = (0.049;\ -0.004)$ have lower negative minima indicating that they are more stable than the other two stable equilibrium points: $(x_0, x_2) = (-0.049;\ -0.049)$ and $(x_0, x_2) = (0.049;\ 0.049)$. Besides that, according to Fig. 6(c), there are seven pseudostable equilibrium points, where the stable/unstable directions are assigned with arrows of different colors. The detail of the potential energy curve (Fig. 6a) helps understanding this analysis. Moreover, there are two unstable equilibrium points, which correspond to the peaks identified in the detail of Fig. 6(a) associated with two unstable directions. Figure 6(d) shows the respective basin of attraction.

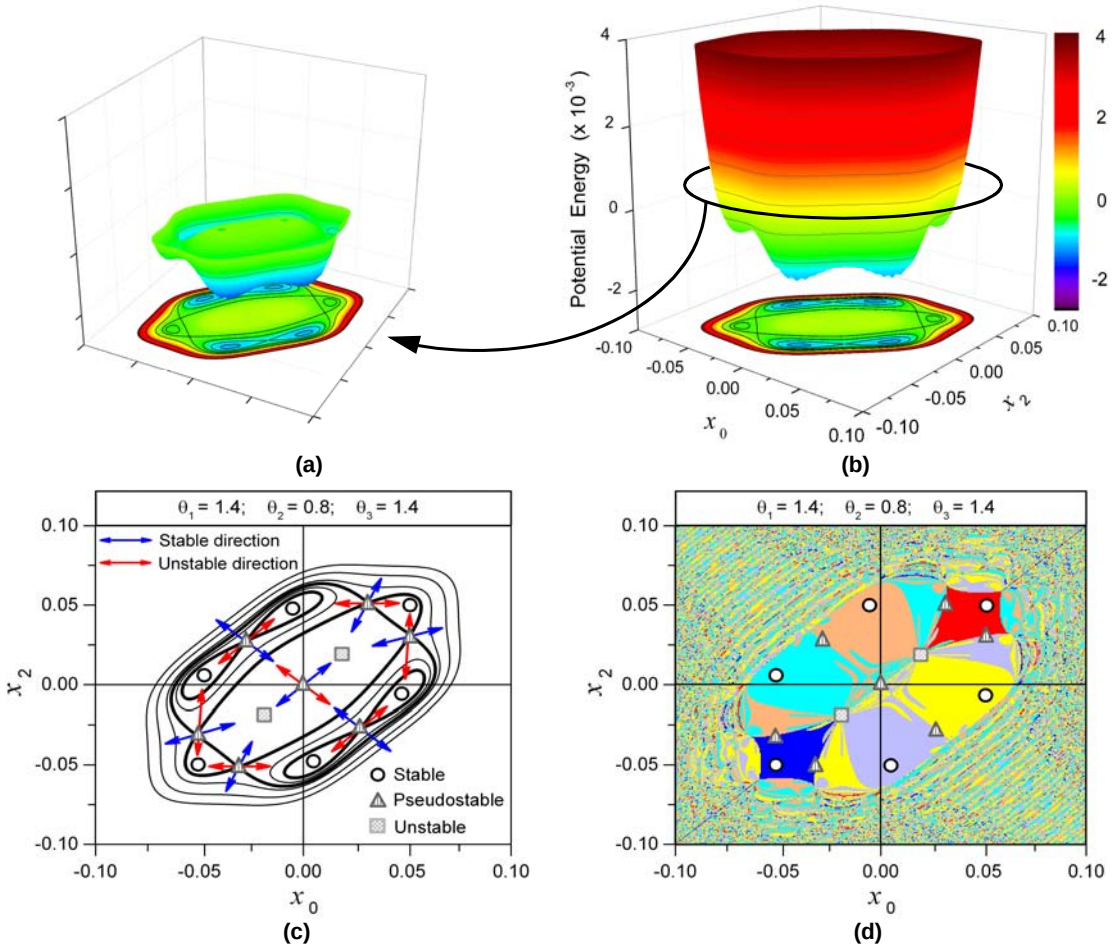

Figure 6 – Stability analysis for a fixed SMA elements condition $\theta_1 = 1.4$; $\theta_2 = 0.8$; $\theta_3 = 1.4$. (a) Detail of potential energy surface; (b) Potential energy × displacements diagram; (c) Conservative state-space orbits; (d) Basins of attraction.

CONCLUDING REMARKS

This paper presents the free-response stability analysis of a 2-DOF **SMA** oscillator, using polynomial model to describe the thermomechanical behavior of **SMAs**. The numerical results for equilibrium points, potential energy surface, conservative state-space orbits and non-conservative basins of attraction are correlated, helping understanding the overall system dynamics. Besides, basins of attraction evolution analyses are performed, varying the spatially distributed **SMA** elements temperature. This work may serve as basis for a further work, concerning nonlinear position control of an actuator with such physical model configuration.

ACKNOWLEDGMENT

The authors would like to acknowledge the support of the Brazilian Research Agencies CNPq, CAPES, FAPERJ as well as INCT-EIE (National Institute of Science and Technology - Smart Structures in Engineering). The acknowledgement also applies to Air Force Office of Scientific Research (AFOSR).

REFERENCES

Achenbach, M. & Muller, I.A.; 1982; "A Model for Shape Memory"; Journal de Physique; Vol. 12; N. 43; pp. 163–167.

Bernardini, D. & Pence, T.J.; 2002; "Models for One-variant Shape Memory Materials Based on Disipation Functions"; International Journal of Non-Linear Mechanics; Vol. 37; N.8; pp. 1299–1317.

Bernardini, D. & Rega, G.; 2005; “Thermomechanical Modelling, Non-linear Dynamics and Chaos in Shape Memory Oscilators”; Mathematical and Computer Modelling of Dynamical Systems; Vol. 11; N. 3; pp. 291–314.

Bernardini, D. & Rega, G.; 2011; “Chaos Robustness and Strength in Thermomechanical Shape Memory Oscillators Part II: Numerical and Theoretical Evaluation”; International Journal of Bifurcation and Chaos; Vol. 21; N. 10; pp. 2783–2800.

Bernardini, D. & Vestroni, F.; 2000; “Hysteretic Modeling of Shape Memory Alloy Vibration Reduction Devices”; Journal of Materials Processing and Manufacturing Science; Vol. 9; N. 2; pp. 101–112.

Bernardini, D. & Vestroni, F.; 2003; “Non-isothermal Oscillations of Pseudoelastic Devices”; International Journal of Non-Linear Mechanics; Vol. 38; pp. 1297–1313.

Boyd, J. & Lagoudas, D.C.; 1996; “A Thermodynamical Constitutive Model for Shape Memory Materials. Part I. The Monolithic Shape Memory Alloy; International Journal of Plasticity; Vol. 12; N. 6; pp. 805–842.

Brinson, L.C., 1993, “One Dimensional Constitutive Behavior of Shape Memory Alloys: themomechanical derivation with non-constant material functions and redefined martensite internal variable”, Journal of Intelligent Material Systems and Structures, Vol. 4, pp. 229–242.

Carpineto, N.; Lacarbonara, W. & Vestroni, F.; 2014; “Hysteretic Tuned Mass Dampers for Structural Vibration Mitigation”; Journal of Sound and Vibration; Vol. 333; pp. 1302–1318.

Cisse, C.; Zaki, W. & Zineb, T.B.; 2016; “A Review of Constitutive Models and Modeling Techniques for Shape Memory Alloys”; International Journal of Plasticity; Vol. 76; pp. 244–284.

Enemark, S.; Savi, M.A. & Santos, I.F; 2014; “Nonlinear Dynamics of a Pseudoelastic Shape Memory Alloy System – Theory and Experiment”; Smart Material and Structures; Vol. 23; Article ID 085018; 17 pp.

Falk, F.; 1980; “Model Free-energy, Mechanics and Thermodynamics of Shape Memory Alloys”; ACTA Metallurgica; Vol. 28; pp. 1773–1780.

Fremond, M.; 1987; “Matériaux à Mémoire de Forme”; *C.R. Acad. Sc. Paris*; Vol. II, N. 7; pp. 239–244.

Ivshin, Y. & Pence, T.J.; 1994; “A Thermomechanical Model for a One Variant Shape Memory Material”; Journal of Intelligent Material Systems and Structures; Vol. 5; pp. 455-473.

Lacarbonara, W. & Vestroni, F.; 2012; “Nonlinear Phenomena in Hysteretic Systems”; Procedia IUTAM: Vol. 5; pp. 69–77.

Lagoudas, D.C., Khan, M.M., Mayes, J.J. & Henderson, B.K.; 2004; “Pseudoelastic SMA Spring Elements for Passive Vibration Isolation: Part II - Simulations and Experimental Correlations”; Journal of Intelligent Material Systems and Structures; Vol. 15; N. 6; pp. 443–470.

Litak, G.; Bernardini, D.; Syta1, A.; Rega, G. & Rysak, A.; 2013; “Analysis of Chaotic Non-isothermal Solutions of Thermomechanical Shape Memory Oscillators”; European Physical Journal Special Topics; Vol. 222; N. 7, pp. 1637–1647.

Machado, L.G.; Lagoudas, D.C. & Savi, M.A.; 2009; “Lyapunov Exponents Estimation for Hysteretic Systems”; International Journal of Solids and Structures; Vol. 46; pp. 1269–1286.

Machado, L.G.; Savi, M.A. & Pacheco, P.M.C.L.; 2003; “Nonlinear Dynamics and Chaos in Coupled Shape Memory Oscillators”; International Journal of Solids and Structures; Vol. 40; N. 19; pp. 5139–5156.

Oliveira, H.S.; de Paula, A.S. & Savi, M.A; 2014; “Dynamical Jumps in a Shape Memory Alloy Oscillator”; Shock and Vibration; Article ID 656212; 10 pp.

Paiva, A.; Savi, M.A.; Braga, A.M.B.; Pacheco, P.M.C.L.; 2005; “A Constitutive Model for Shape Memory Alloys Considering Tensile-compressive Asymmetry and Plasticity. International Journal of Solids and Structures; Vol. 42; N. 11-12; pp. 3439–3457.

Piccirillo, V.; Balthazar, J.M.; Tusset, A.M.; Bernardini, D & Rega, G.; 2015; “Non-linear Dynamics of a Thermomechanical Pseudoelastic Oscillator Excited by Non-ideal Energy Sources”; International Journal of Non-Linear Mechanics”; Vol. 77; pp. 12–27.

Rodrigues, G.V., Paiva, A. & Fonseca, L.M.; 2015; “Nonlinear Investigation of Chaos and Hyperchaos in a 2-DOF Shape Memory Oscillator”; Proceedings of 23rd ABCM International Congress of Mechanical Engineering; 8 pp.

Santos, B.C. & Savi, M.A.; 2009; “Nonlinear Dynamics of a Nonsmooth Shape Memory Alloy Oscillator”; Chaos, Solitons and Fractals; Vol. 40; pp. 197–209.

Savi, M.A.; De Paula, A.S. & Lagoudas, D.C.; 2011; “Numerical Investigation of an Adaptive Vibration Absorber Using Shape Memory Alloys” Journal of Intelligent Material Systems and Structures; Vol. 22; pp. 67–80.

Savi, M.A.; Sa, M.A.N.; Paiva A. & Pacheco, P.M.C.L.; 2008; “Tensile-compressive Asymmetry Influence on Shape Memory Alloy System Dynamics”; Chaos, Solitons and Fractals; Vol. 36; pp. 828–842.

Seelecke, S.; 2002; “Modeling the Dynamic Behavior of Shape Memory Alloys”; International Journal of Nonlinear Mechanics; Vol. 37; N. 8; pp. 1363–1374.

Silva, L.C.; Savi, M.A. & Paiva, A.; 2013; “Nonlinear Dynamics of a Rotordynamic Nonsmooth Shape Memory Alloy System”; Journal of Sound and Vibration; Vol. 332; pp. 608–621.

Sitnikova, E.; Pavlovskaia E. & Wiercigroch, M.; 2008; “Dynamics of an Impact Oscillator with SMA Constraint”; European Physical Journal Special Topics; Vol. 165; pp. 229–238.

Sitnikova, E.; Pavlovskaia, E.; Ing, J. & Wiercigroch, M.; 2012; “Suppressing Nonlinear Resonances in an Impact Oscillator Using SMAs”; Smart Material and Structures; Vol. 21; Article ID 075028; 16pp.

Savi, M.A.; 2015; “Nonlinear Dynamics and Chaos in Shape Memory Alloy Systems”; International Journal of Non-Linear Mechanics; Vol. 70; pp. 2–19.

Savi, M.A. & Braga, A.M.B.; 1993; “Chaotic Vibrations of an Oscillator with Shape Memory”; Journal of the Brazilian Society of Mechanical Sciences; Vol 15; N. 1; pp. 1–20.

Savi, M.A. & Pacheco, P.M.C.L.; 2002; “Chaos and Hyperchaos in Shape Memory Systems”; International Journal of Bifurcation and Chaos; Vol. 12; N. 3; pp. 645–657.

RESPONSIBILITY NOTICE

The authors are the only responsible for the printed material included in this paper.